

# Why are mixed-phase altocumulus clouds poorly predicted by large-scale models? Part II: Vertical resolution sensitivity and parameterization

Andrew I. Barrett,<sup>1</sup> Robin J. Hogan<sup>1</sup> and Richard M. Forbes<sup>2</sup>

**Abstract.** Single-column model simulations of mixed-phase altocumulus clouds were shown to have a strong vertical-resolution sensitivity in Part I of this paper with coarse resolution models unable to simulate the long-lived supercooled liquid layer at cloud top, typically only 200 m thick. In this paper the sensitivity to vertical resolution is investigated using idealized simulations. We find that the vertical-resolution sensitivity results from unrepresented vertical gradients of ice water mixing ratio and temperature near cloud top, which creates errors in the calculation of mixed-phase microphysical process rates and diagnosis of thin liquid water layers. As a result the liquid water layer becomes quickly glaciated and altocumulus cloud lifetime is underestimated.

A novel parameterization is introduced that accounts for the vertical gradients of ice water mixing ratio and temperature in the microphysics calculations and the diagnosis of liquid cloud near cloud top. It substantially improves the representation of altocumulus layers in coarse vertical-resolution single-column model simulations and reduces the bias identified in Part I. Applying the new parameterization to simulations of the 21 observed study days from Part I completely removes the large underestimate in supercooled water content warmer than  $-30^{\circ}\text{C}$ . Given the radiative importance of mixed-phase altocumulus clouds, their underestimation by NWP models and their potential to act as a negative climate feedback there is a need to re-evaluate the global climate sensitivity by implementing the findings in these two papers in a climate model.

## 1. Introduction

Mid-latitude mixed-phase altocumulus clouds have a thin layer of supercooled liquid water at cloud top above a region of falling ice particles [Hobbs and Rangno, 1985; Rauber and Tokay, 1991]. Physically similar mixed-phase stratocumulus exists in polar regions [Morrison *et al.*, 2012]. These clouds reflect more incoming solar radiation than clouds containing only ice particles due to the layer of supercooled liquid water near cloud top [Hogan *et al.*, 2003]. Furthermore, they can exist for long periods [Shupe *et al.*, 2006] with the thin liquid water layer at cloud top that slowly produces ice particles. An increase in the amount of cloud in the mid-latitude mid-levels and lower-level polar clouds as predicted by some climate models [Tsushima *et al.*, 2006] would constitute a negative climate feedback [Mitchell *et al.*, 1989; Senior and Mitchell, 1993]. However, we can have little confidence in the predicted magnitude of these changes when the representation of mixed-phase clouds in most models is still very crude.

The frequency of persistent supercooled liquid or mixed-phase clouds are substantially underestimated by many weather and climate models [Barrett *et al.*, 2014; Zhang *et al.*, 2005]. Part I of this paper [Barrett *et al.*, 2014] reports that simulations of mixed-phase altocumulus exhibit a sensitivity to a number of factors including the specification of the mixed-phase microphysics, but also the vertical-spacing of model levels (hereafter resolution). Single-column model

simulations of thin altocumulus layers over 21 days showed that simulations with coarse vertical resolution (500 m) had just 5% the supercooled liquid water content of the same days simulated by the same model with fine resolution (50 m). The typical vertical resolution of GCMs is close to or coarser than the coarsest resolution (500 m) analyzed in Part I and with such a large sensitivity to the model vertical resolution, the coarseness of GCM resolution may be a large factor in their severe underestimate of mid-level cloud occurrence found in Part I, Illingworth *et al.* [2007] and Zhang *et al.* [2005]. Given these layers are typically only a few hundred metres thick [Hogan *et al.*, 2003] this sensitivity is not surprising, but the exact mechanisms causing the underestimate have not previously been described.

Climate models typically have a coarser vertical resolution in the mid-troposphere than state-of-the-art weather prediction models and therefore likely suffer even more from the lack of supercooled liquid layers. The absence of optically thin and moderate clouds from climate models [Zhang *et al.*, 2010], and the resulting radiative errors, may be altering their predictions of future climate. The representation of clouds and cloud feedbacks are the largest cause of uncertainty in future climate projections [Andrews *et al.*, 2012; Bony *et al.*, 2006]. It is therefore important to understand and correct for this vertical resolution sensitivity in climate models and to revise our estimate of climate sensitivity.

We perform this study to understand why models show this large vertical resolution sensitivity and to develop a parameterization that allows mixed-phase layer clouds to be represented in models in a resolution-independent way. This paper reports on mixed-phase cloud properties in single-column model simulations where the vertical resolution is varied from 50-m to 500 m. To determine which processes are contributing to the vertical resolution sensitivity we individually modify four processes in the high-resolution simulations such that they behave as if they were in a coarse-resolution model. This means that they take inputs averaged over 500-m and give outputs at 500-m resolution.

<sup>1</sup>Department of Meteorology, University of Reading, UK.

<sup>2</sup>European Centre for Medium-Range Weather Forecasts, Reading, UK.

Additionally, the process rates of the microphysics scheme are analyzed to highlight their role in the vertical resolution sensitivity.

Section 2 briefly describes the numerical model used and section 3 details the magnitude of the vertical resolution sensitivity found using this model. A parameterization is developed in section 4 that accounts for the vertical gradients of ice water mixing ratio and temperature near the cloud top. The performance of this parameterization is then demonstrated within the model across a large range of vertical resolutions in section 5. A discussion of the key results and implications is in section 6.

## 2. Vertical resolution sensitivity

### 2.1. Numerical model description and setup

The numerical model used for these experiments is EMPIRE (Evaluate Mixed-Phase Importance in Radiative Exchange), which is described fully in Part I of this paper. This model is a single-column model designed to be similar to GCMs commonly used for numerical weather prediction and climate simulation. Compared to a GCM, this model is very flexible and enables quick and efficient experiments to determine the importance of physical processes and model configuration on cloud evolution. For example, this allowed us to determine that mixed-phase altocumulus cloud lifetime and supercooled liquid water content was very much dependent on the specification of ice growth by deposition in the model [Barrett *et al.*, 2014].

The configuration of EMPIRE used for this study includes all physics parameterizations described in Part I. These include: mixed-phase microphysics [Wilson and Ballard, 1999], sub-grid cloud scheme [Smith, 1990], two-stream radiation [Edwards and Slingo, 1996], the ‘stratocumulus cloud-top cooling’ part of the Lock *et al.* [2000] non-local boundary layer scheme for turbulent mixing in the vertical, and the Louis [1979] scheme for ‘local’ turbulent mixing. The advective tendencies and vertical velocities are set to zero during all idealised simulations described in this paper.

The vertical model-levels in EMPIRE are equally spaced throughout the depth of the model with a model top at 12.5 km. The vertical spacing of these model-levels is specified for each simulation with values between 50 and 500 m.

For the experiments described below, the 50-m resolution model is initialized with data from the 0600 UTC 5 September 2003 radiosonde ascent at Larkhill, UK, when a supercooled altocumulus layer was present with the cloud top at  $-20^{\circ}\text{C}$ . The model is then run forward for 1 hour to allow the ice phase of the cloud to come to an approximate equilibrium. At one hour into the simulation the model prognostic

variables ( $\theta_L$ ,  $q_t$ ,  $q_i$ ,  $u$ ,  $v$ ) are linearly interpolated to the required model resolution and the model continues running at the new resolution for a further three hours. Simulations are run at fine resolution (50 metres model-level spacing) to coarse resolution (500 metres) and at each 25 metre interval between.

The results reveal a substantial reduction of liquid water path at coarse resolutions (Fig. 1). Simulations with a vertical resolution of 100 m or finer are able to sustain a supercooled liquid water layer at cloud top (with liquid water path greater than  $1 \text{ g m}^{-2}$ ) for at least 3 hours, whereas in coarser resolution simulations the liquid water layer is removed rapidly (within 30 minutes for simulations with vertical resolution coarser than 325 m). There exists a notable vertical resolution sensitivity even for simulations with resolution at or finer than 100 m where the liquid water path varies by up to a factor of 2 after 3 hours of the simulation; however, the liquid layer persists for at least 3 hours in each of these simulations.

The contrast between fine and coarse resolution simulations is illustrated in figure 3 where time-height plots of ice and liquid water contents are presented from the 50-m and 500-m simulations. A persistent liquid water layer is present at the top of the cloud layer in the 50-m simulation which persists for the duration of the 3-hour simulation (Fig. 3b). The cloud layer initially has a liquid water path of  $11.5 \text{ g m}^{-2}$ , which equates to a cloud depth of 200 m if the layer were adiabatic and a depth of 400 m in the model as some of the liquid water is present in the inversion layer. This layer gradually thins and the liquid water path of the layer decreases to  $2.6 \text{ g m}^{-2}$  after 3 hours of the simulation. The liquid layer is continually producing ice (Fig. 3a) in small concentrations near cloud top but the ice water mixing ratio decreases further below cloud top as the ice particles grow larger and fall into unsaturated air. In contrast, the 500-m simulation has a short-lived liquid water layer at cloud top that persists for only 30 minutes (Fig. 3d), with a rapidly decreasing liquid water path. Throughout this time period the ice water mixing ratio near cloud top is rapidly increasing (Fig. 3c). High ice concentrations in the water-saturated region near cloud top promote rapid growth of ice particles, which quickly depletes the supercooled liquid water present. The high ice water mixing ratio values move lower in the cloud layer later in the cloud lifetime as the source of new ice particles at cloud top (the liquid water layer above) has been removed. Gradually the ice water mixing ratio values also decrease as the ice particles fall into unsaturated air and are not replaced by new particles from above and by the end of the 3 hour simulation the ice water path has decreased to  $6.1 \text{ g m}^{-2}$ . This depletion of both liquid and ice from the cloud layer will result in a substantial

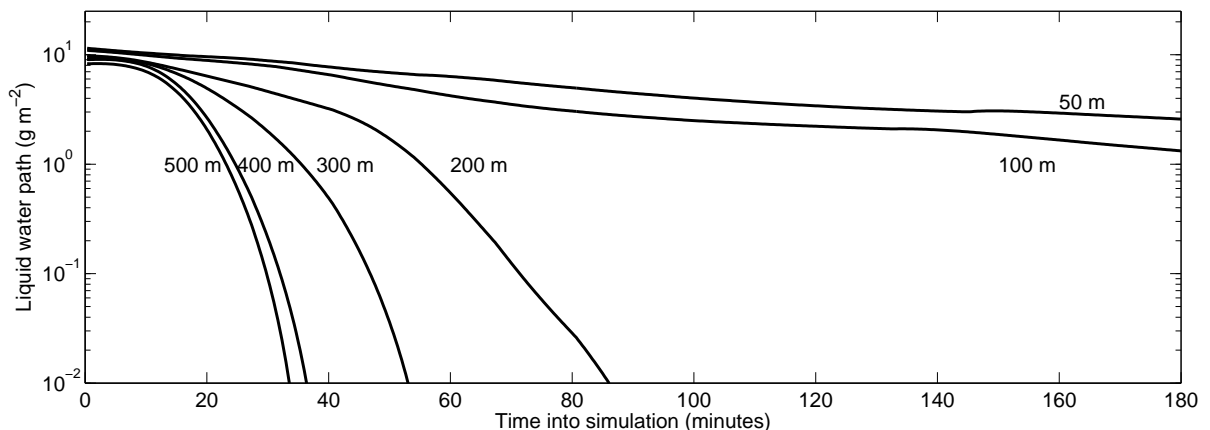


**Figure 1.** The evolution of simulated liquid water path with time for model vertical resolutions of 50–500 m.

difference in the radiative properties of the cloud compared to the 50-m simulation.

## 2.2. Role of key processes

The large sensitivity to vertical resolution presented above must stem from at least one process with a vertical resolution sensitivity. To identify where this sensitivity comes from we run further simulations at 50 metre vertical resolution but in each simulation one process is modified to act on data averaged to 500 metre resolution. This is designed to mimic the behaviour of that process in the 500-m resolution simulation, but retaining finer resolution information for each of the other processes. The process that is modified is different in each simulation and this allows for the identification of the processes that are most sensitive to vertical resolution. The processes degraded in the simulations were:

1. calculation of ice growth rate and fall speed,
2. conversion of  $\theta_L$  and  $q_t$  to  $T$ ,  $q$  and  $q_t$ ,
3. diagnosis and implementation of vertical turbulent mixing,
4. radiative transfer.

The input data for the degraded process is calculated by averaging the relevant properties over 10 model levels from the 50-m simulation that correspond to nearest 500-m model level. The output from these processes are applied equally to each of the 10 model levels.

The liquid and ice water mixing ratios from these four simulations are shown together with the 50-m and 500-m resolution simulations for comparison in figure 3. The first two rows show the 50-m and 500-m resolution simulations. The third to sixth row show the simulations with one process degraded; the process degraded is described on the left of the figure.

The degradation of the ice microphysics scheme to 500-m resolution results in an increased ice water mixing ratio near cloud top during the first hour of the simulation (Fig. 3e) similar to the 500-m resolution simulation (Fig. 3c) but with lower ice water mixing ratio values. The liquid water content in the same simulation decreases rapidly with time (Fig. 3f) due to the greater production of ice near the cloud

top. The liquid layer persists for longer than the 500-m simulation but this is largely due to being able to resolve low liquid water contents in this layer with the 50-m resolution.

The ‘Diagnosing Liquid’ simulation reduces the resolution of data passed to the cloud scheme such that it acts on values of  $\theta_L$ ,  $q_t$ ,  $p$  that have been averaged over a 500-m layer. Simulations in which the cloud properties ( $q_l$ ,  $q_v$ , cloud fraction and temperature) are calculated in this way had a much reduced liquid water content at cloud top (Fig. 3h) compared to the 50-m simulation. Again the liquid water layer is removed more quickly in this simulation than the 50-m simulation. In this simulation the ice water mixing ratio near cloud top is very similar to the 50-m simulation; however, the ice water mixing ratio beneath the top 500-m of the cloud layer is increased relative to the 50-m simulation.

The degrading of the turbulent mixing near cloud top is achieved by averaging the input profiles of temperature and wind speeds to 500 metre resolution, performing the calculations using this 500-m data and then applying the diagnosed diffusivity profiles to the 50-m resolution model. This averaging process reduced the amount of mixing in the simulations because the model often did not diagnose any sufficient instability on the 500-m averaged data to initiate turbulent mixing. The degrading of the turbulent mixing results in a thinner liquid water layer but with higher liquid water content values (Fig. 3j) than the 50-m simulation. The liquid water path at the end of the simulation is within  $0.5 \text{ g m}^{-2}$  of the starting value whereas the control 50-m simulation the liquid water content decreases by  $9 \text{ g m}^{-2}$ . This change is due to the reduced mixing of radiatively cooled air near the top of the cloud layer with warmer air lower down, which results in a narrower, colder layer of air that contains more liquid water at cloud top. The ice water mixing ratio is slightly reduced by the end of the simulation (Fig. 3i), but this process is certainly not the cause of the large vertical resolution sensitivity as it is of smaller magnitude and opposite sign of the overall effect.

Changing the radiative transfer calculations to act on data averaged to 500-m resolution results in lower liquid water contents throughout the simulation (Fig. 3l) due to a reduction in the rate of longwave cloud top cooling diagnosed by the radiation scheme. The ice water mixing ratio

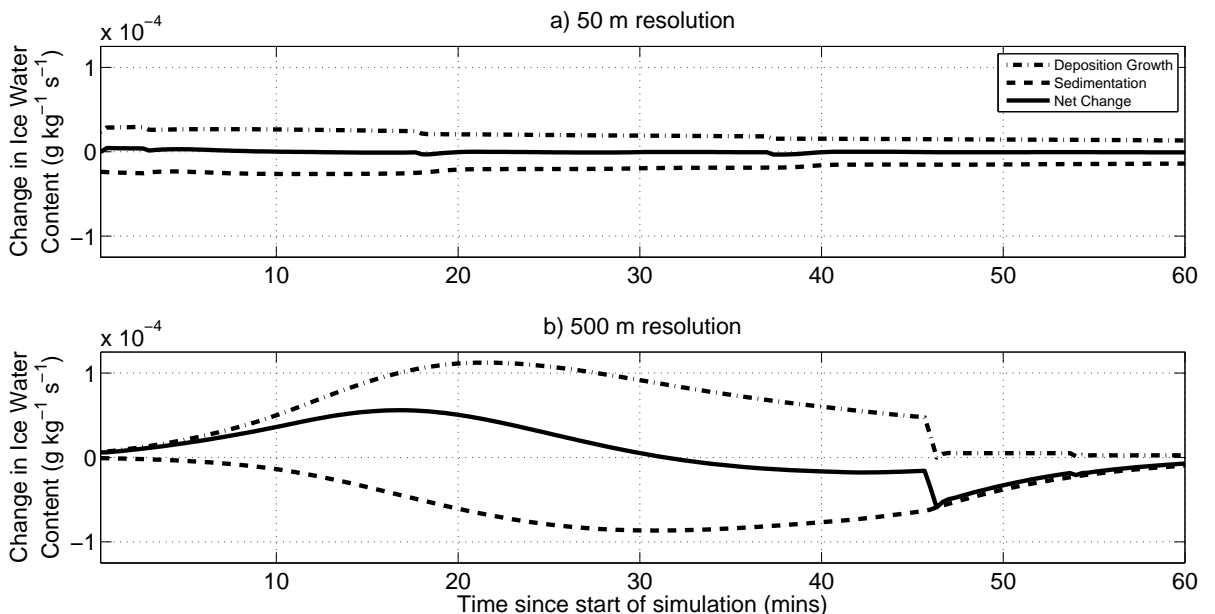


**Figure 2.** Time series of the rate of production and sedimentation of ice at resolutions of a) 50 m and b) 500 m.

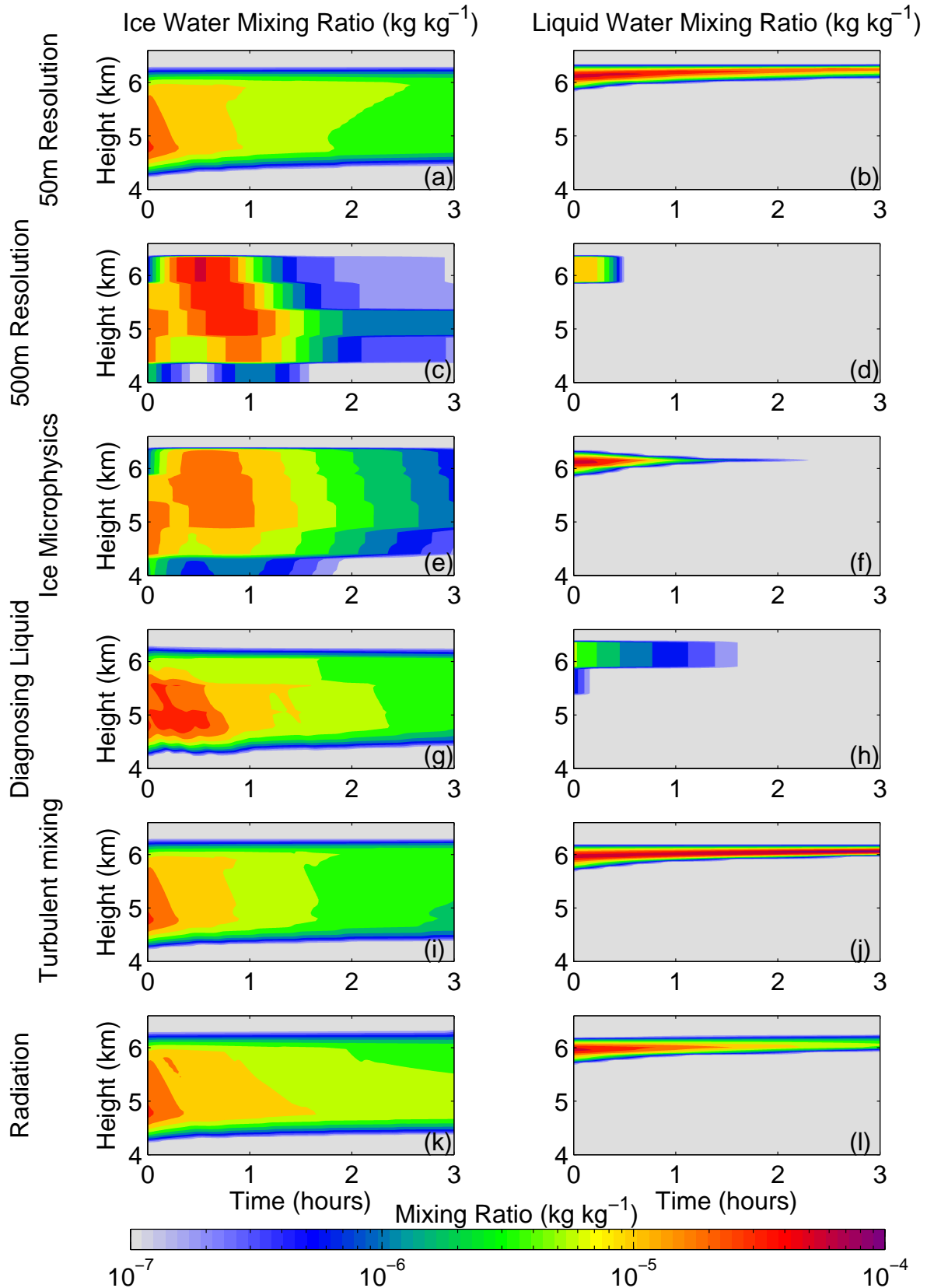


**Figure 3.** Liquid and ice water mixing ratios from six idealized EMPIRE simulations. The simulations are: (a-b) 50-m resolution, (c-d) 500-m resolution, (e-f) 50-m resolution with ice microphysical processes averaged across 10 model levels, (g-h) 50-m resolution where the temperature is averaged over a 500-m layer before calculating cloud properties, (i-j) 50-m resolution with turbulent mixing calculated on a 500-m grid, and (k-l) 50-m resolution with the radiation scheme using 500-m averaged quantities.

decreases more slowly with time (Fig. 3k) resulting in an ice water path that is 50% larger by the end of the 3 hour simulation than the control simulation. The vertical structure also changes, with the largest ice water mixing ratio values now found near the cloud base rather than top (Fig. 3k).

The changes in the latter 2 experiments are somewhat smaller than those experienced by the degradation of either ice microphysics or diagnosis of liquid water. This set of simulations show that two of the processes contribute strongly to the vertical resolution sensitivity. Both the ice microphysics and the detection of liquid water are sensitive to the

vertical resolution of the model. The two simulations where the processes of microphysics and diagnosing liquid water are modified both result in a collapse of the supercooled liquid layer within the first hour of the simulation (Fig. 3 f, h) similar to the 500-m simulation (Fig. 3c).

### 2.3. Ice microphysics non-convergence and process rates

The ice microphysics is the major source of non-convergence as the resolution of the simulations increase.

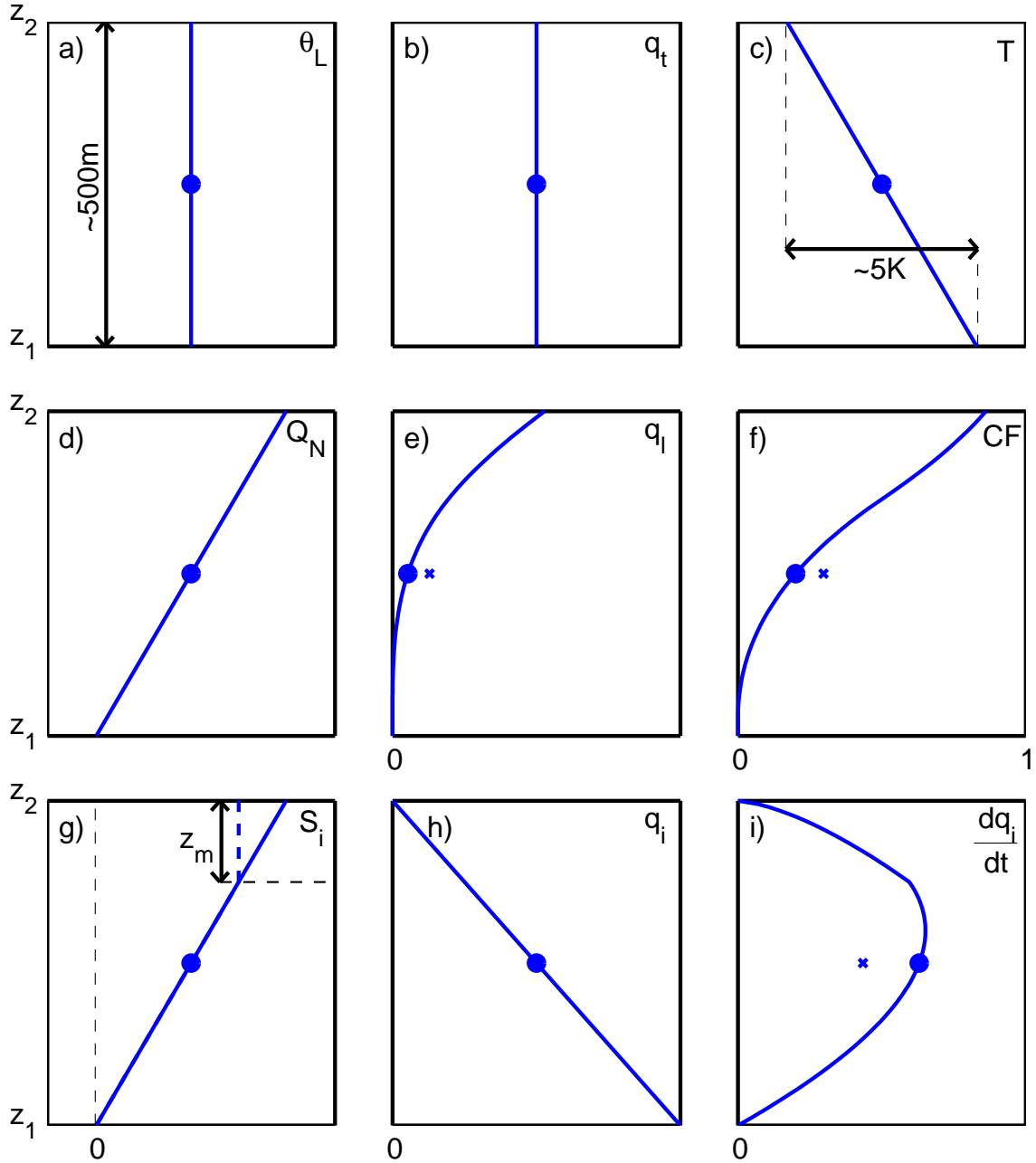


**Figure 4.** Typical vertical profiles from the upper 500-m of a mixed-phase altocumulus layer (lines) and equivalent values calculated using the 500-m vertical average of the prognostic variables ( $\theta_L$ ,  $q_t$  and  $q_i$ ) of the model (dots). Where the calculated value differ from the true mean of the layer the true mean is marked by a cross. The profiles are for a) liquid water potential temperature, b) total water mixing ratio, c) temperature, d)  $Q_N$  from the cloud scheme (defined in eq. 19), e) liquid water mixing ratio, f) liquid cloud fraction, g) supersaturation with respect to ice, h) ice water mixing ratio, i) rate of ice growth due to vapour deposition.

To further understand why this occurs we investigate the rate of production of ice within a 500-m layer at cloud top and the sedimentation rate of ice out of the bottom of that layer. These two terms are plotted for 50 and 500-m resolution simulations in figure 2. The ice production term includes the effects of nucleation (a small contribution), ice particle growth by vapour deposition (a large contribution) and the collection of liquid water by falling ice particles (almost negligible). The 50-m simulation is close to equilibrium at the start, with the rate of ice production almost balancing the rate of ice loss through sedimentation, resulting in a near zero net change. This approximate balance is maintained throughout the simulation, although the magnitudes of each term decrease slowly as the available water vapour in the cloud is used up by the production of ice. In contrast the 500-m simulation has a much larger production rate of ice that develops in the first few minutes of the simulation and also a slower initial rate of loss due to sedimentation. The rate of production of ice in the 500-m simulation peaks about 20 minutes into the simulation, after which time it has used up much of the available water vapour in the cloud layer. The sedimentation term becomes larger, resulting in a negative net change of ice water mixing ratio. Eventually, after around 45 minutes, the ice production has removed all available vapour within the cloud layer. At this point the ice production falls to almost zero but the sedimentation rate of ice is still quite large. This imbalance results in a rapid collapse of the cloud as ice falls out of the layer.

### 3. Parameterization of sub-grid cloud vertical structure

The different behaviours of the ice microphysical process rates in these clouds appears to stem from vertical gradients near the cloud top that are not resolved by the coarse resolution simulation. A schematic of typical vertical profiles within the upper 500-m of the cloud are sketched in Fig. 4. These show that there are considerable vertical gradients present, particularly of temperature (Fig. 4c), ice water mixing ratio (Fig. 4h) and supersaturation with respect to ice (Fig. 4g). The temperature decreases with height throughout the cloud layer due to the decrease in air pressure from bottom to top. The layer is usually well-mixed by turbulence generated from cloud top radiative cooling, so the potential temperature and total water mixing ratio are near-constant with height. The ice water mixing ratio increases with distance from cloud top, with a value of zero at the top of the cloud. The supersaturation with respect to ice decreases with distance from cloud top and is controlled by the change in temperature over the layer. Similarly, the liquid water layer is confined to the top of the layer, where the air is coldest and decreases with distance away from cloud top. The fact that the 500-m simulation has only one value for each prognostic variable means that it is unable to resolve these vertical gradients and this is the cause of the resolution sensitivity in the ice microphysics.

The previous section described that the vertical resolution sensitivity arises from neglecting the vertical gradients of temperature, liquid and ice water mixing ratios within a single model layer near cloud top. The gradients are important when determining the ice microphysical processes rates.

Most of the ice production in altocumulus clouds happens due to vapour deposition which occurs because the air is supersaturated with respect to ice. The rate of growth of an individual ice particle can be calculated following Pruppacher and Klett [1978] as

$$\frac{dm}{dt} = \frac{4 \pi C F S_i}{\left(\frac{L_s}{R_v T} - 1\right) \frac{L_s}{K T} + \frac{R_v T}{e_i(T) D}} \quad (1)$$

where  $m$  is the mass of the ice particle,  $C$  is the capacitance of the ice particle, dependent on its size and shape,  $F$  is the ventilation coefficient,  $S_i$  is the supersaturation of the air with respect to ice,  $L_s$  is the latent heat of sublimation,  $K$  is the thermal conductivity of air,  $D$  is the diffusivity of water vapour in air and  $e_i$  is the saturated vapour pressure over ice. Following Wilson and Ballard [1999], we use a ventilation coefficient, computed as  $F = 0.65 + 0.44 \text{Sc}^{1/3} \text{Re}^{1/2}$  [Pruppacher and Klett, 1978] with the Schmidt number ( $\text{Sc} = 0.6$ ) and the Reynolds number ( $\text{Re} = v(D)\rho D/\mu$ ) where  $v(D)$  is the fall-speed of the ice particle and  $\mu$  is the dynamic viscosity of air.

The model calculates the depositional growth of ice for all ice particles within a grid-box. This requires integrating (1) over an assumed size distribution. For an inverse-exponential size distribution with intercept parameter  $N_0$  (such as that from Wilson and Ballard [1999]) this gives:

$$\frac{dq_i}{dt} = \frac{2\pi F S_i}{A} \left(\frac{N_0}{\rho}\right)^{1-\frac{2}{b+1}} \left(\frac{q_i}{a\Gamma(b+1)}\right)^{\frac{2}{b+1}}, \quad (2)$$

where the time rate of change of the ice water mixing ratio ( $q_i$ ) is given in terms of the supersaturation with respect to ice ( $S_i$ ), the intercept parameter of the ice particle size distribution ( $N_0 = 2 \times 10^6 \exp(-0.1222T)$ ), the air temperature ( $T$ ) and density ( $\rho$ ),  $a$  and  $b$  from the ice mass-diameter relationship ( $m = aD^b$ ), and  $A$  is the denominator of (1).

The rate of ice growth by vapour deposition calculated using (2) is a function of the product of the ice water mixing ratio and the supersaturation with respect to ice. Both have a sizable vertical gradient near cloud top, but of opposite sign (Fig. 4g,h). The resulting product of these quantities is not a linear function of height, and choosing the value from the middle of the layer as a representative value of the whole layer results in considerable overestimate of the true layer-mean ice growth rate (Fig. 4i).

#### 3.1. Parameterization overview

We now introduce a parameterization for the vertical structure of the ice water mixing ratio and temperature that can be applied at cloud top in a numerical model. To do so requires making four assumptions about the properties of the cloud layer. The following four assumptions apply only to the upper-most mixed-phase model-level:

1. The ice-phase of the cloud fills at least this model-level, with cloud top at the model-level top.
2. Ice water mixing ratio increases linearly with distance from cloud top, with zero at the model-level top and  $2\bar{q}_i$  at the model-level bottom.
3. The layer is well mixed, and hence  $d\theta_L/dz$  and  $dq_t/dz$  are both zero.
4. Diagnosed quantities (e.g. temperature, supersaturation with respect to ice) vary linearly with height throughout the grid-box.

We use these assumed profiles to calculate the rate of ice growth by deposition, the sedimentation of cloud ice from the model level at cloud top to the one below, and to calculate the liquid water content and cloud fraction within the upper-most mixed-phase model-level. In doing so, we enable coarse vertical resolution models to capture the important vertical gradients near cloud top and more accurately simulate persistent mixed-phase altocumulus clouds.

The third assumption about the layer being well mixed is a result of the turbulent mixing of the layer driven by cloud top radiative cooling and is supported by observations [Morrison *et al.*, 2012; Zuidema *et al.*, 2005; Verlinde *et al.*, 2007]. The linear increase of ice water mixing ratio with distance

from cloud top in the second assumption is supported by remote sensing observations [Shupe *et al.*, 2008], in-cloud observations [Fleishauer *et al.*, 2002; McFarquhar *et al.*, 2007], large-eddy modelling studies [Smith *et al.*, 2009] and analysis of EMPIRE model simulations.

To apply the parameterization of vertical structure at cloud top we need to determine in which grid-boxes it should be active. This first requires determining the top of mixed-phase layer clouds and then deciding over what depth within the cloud to use the parameterization. We determine the presence of mixed-phase layer clouds when the following criteria are met:

1.  $q_l > 10^{-7} \text{ kg kg}^{-1}$
2.  $q_i > 10^{-10} \text{ kg kg}^{-1}$
3.  $-40^\circ\text{C} < T < 0^\circ\text{C}$ .

The parameterization is then applied in the highest model level of each distinct cloud layer that meets this criteria. However, if the second-highest model level also meets the criteria, but has at least five times more liquid than the highest model level, the parameterization is applied in the second-highest model level instead. This helps to remove ‘‘jumpiness’’ in the simulations when small quantities of liquid are present above the main cloud layer. The parameterization is only applied in a single model level, regardless of the resolution of the model at that height. This may result in some resolution dependence of the solution but has the advantage that it is much simpler to apply. Additionally, as model resolution increases we expect the higher resolution of the model to better resolve the vertical structure near cloud top and reduce the requirement for the parameterization. The results shown in the testing section below demonstrate that this method does give almost resolution independent results and the added complications of applying the parameterization over a fixed depth are not required.

The parameterization is applied only to the upper-most mixed-phase model-level of each cloud layer. For coarsely spaced model-levels this allows for the representation of the vertical gradient near the cloud top, whereas for finely spaced model-levels it allows the model to resolve the cloud vertical structure without much impact from the parameterization. The parameterization scales the ice growth rate and sedimentation rate calculated by the model so that it is equivalent to the correct value if the vertical gradients of  $S_i$  and  $q_i$  within the model-level were explicitly resolved.

### 3.2. Correcting ice growth rate

All the quantities in (2) are ordinarily assumed to be constant with height within a model grid-box. We correct for this by assuming a vertical profile for horizontally averaged  $S_i$  and  $q_i$  (see figure 4). The temperature also changes with height, and will affect  $A$ ,  $T$  and  $\rho$  in (2); however, the fractional changes in these terms are much smaller than for  $S_i$  and  $q_i$  and are hence neglected. This allows us to simplify (2) to

$$\frac{dq_i}{dt} = \alpha S_i q_i^{\frac{2}{b+1}}, \quad (3)$$

where

$$\alpha = \frac{2\pi}{A} \left( \frac{N_0}{\rho} \right)^{1-\frac{2}{b+1}} \left( \frac{1}{a\Gamma(b+1)} \right)^{\frac{2}{b+1}} \quad (4)$$

is constant with height under our assumption. If all terms in (3) were constant with height (as typically assumed in model parameterizations), with a value equal to their grid-box mean (denoted by an overbar), then the calculated growth rate would be

$$\widehat{\frac{dq_i}{dt}} = \alpha \overline{S_i} \overline{q_i}^{\frac{2}{b+1}}. \quad (5)$$

Here  $\overline{S_i}$  is the mean model supersaturation defined as

$$\overline{S_i} = \frac{\overline{q_v} - q_{si}(\overline{T})}{q_{si}(\overline{T})}, \quad (6)$$

with  $\overline{q_v}$  being the mean water vapour mixing ratio ( $\overline{q_v} = \overline{q_l} - \overline{q_i}$ ) and  $q_{si}(\overline{T})$  being the water vapour mixing ratio at ice saturation.

The linear increase of  $q_i$  with distance below from cloud top ( $z'$ ) is given by

$$q_i = \frac{2z'}{\Delta z} \overline{q_i}, \quad (7)$$

where  $\Delta z$  is the depth of the grid-box in which the parameterization is being applied.  $S_i$  increases linearly with height as the cloud top is approached, but it may reach a maximum value where if the air becomes entirely liquid saturated and hence  $q_v$  cannot increase further even if  $q_l$  does. This occurs at a distance,  $z_m$ , below the cloud top yielding the below function of height for  $S_i$ :

$$S_i = \begin{cases} \left[ \frac{\Delta z - 2z'}{\Delta z} \beta + 1 \right] \overline{S_i} & \text{if } z' \geq z_m \\ \gamma \overline{S_i} & \text{if } z' < z_m \end{cases} \quad (8)$$

where

$$\beta = \frac{\Delta S_i}{\overline{S_i}} \quad \text{if } \overline{S_i} \neq 0, \quad (9)$$

and

$$\gamma = \frac{(S_i)_a}{\overline{S_i}} \quad \text{if } \overline{S_i} \neq 0. \quad (10)$$

The difference between the supersaturation at the top and base of the grid-box is

$$\Delta S_i = (S_i)_{\text{top}} - (S_i)_{\text{base}}. \quad (11)$$

The maximum supersaturation attainable is

$$(S_i)_a = \frac{q_{sl}(\overline{T})}{q_{si}(\overline{T})} + (1 - \text{RH}_{\text{crit}}). \quad (12)$$

and the parameterized value of  $S_i$  is not allowed to exceed this value. The distance from cloud top over which  $S_i$  is assumed constant with height is calculated as

$$z_m = \Delta z \frac{\overline{S_i} + 0.5\Delta S_i - (S_i)_a}{\Delta S_i} \quad (13)$$

The strength of parameterizing  $q_i$  and  $S_i$  as multiples of  $\overline{q_i}$  and  $\overline{S_i}$  is that the correct growth rate can be calculated from the standard calculated growth rate by a simple multiplicative factor. A problem is encountered if  $S_i$  is zero, however, in this case the calculated grid-box mean growth rate would be zero anyway.

The correct mean ice growth rate in this grid-box can be calculated by integrating equation 3 over the depth of the grid-box using profiles of  $q_i$  and  $S_i$  from (7) and (8) respectively. As  $\alpha$  is assumed to be constant with height, this can be written as

$$\begin{aligned} \overline{\frac{dq_i}{dt}} &= \frac{\alpha}{\Delta z} \int_0^{\Delta z} S_i q_i^{\frac{2}{b+1}} dz. \\ &= \frac{\alpha}{\Delta z} \overline{S_i} \overline{q_i}^{\frac{2}{b+1}} \left\{ \int_0^{z_m} \gamma \left( \frac{2z}{\Delta z} \right)^{\frac{2}{b+1}} dz \right. \end{aligned} \quad (14)$$

$$+ \int_{z_m}^{\Delta z} \left[ \frac{\Delta z - 2z}{\Delta z} \beta + 1 \right] \left( \frac{2z}{\Delta z} \right)^{\frac{2}{b+1}} dz \} \quad (15)$$

After integrating and simplifying terms, this leaves a relatively simple expression

$$\frac{dq_i}{dt} = \left[ \frac{b+1}{2b+1} \left( (1+\beta-\gamma) \left( 1 - \frac{z_m}{\Delta z} \frac{2b+1}{b+1} \right) + \gamma \right) + \beta \frac{2b+2}{3b+2} \left( \frac{z_m}{\Delta z} \frac{3b+2}{b+1} - 1 \right) \right] 2^{\frac{b}{b+1}} \widehat{\frac{dq_i}{dt}}, \quad (16)$$

where  $\widehat{\frac{dq_i}{dt}}$  is the ‘‘regular’’ growth rate calculated by (5). As the parameterized growth rate is related to the regular growth rate by a factor, the correct timestep change of ice mixing ratio can be obtained by multiplying by this factor.

### 3.3. Correcting ice sedimentation rate

The calculation of the rate of change of ice mixing ratio due to sedimentation requires the fluxes of ice both into and out of the layer. These fluxes require values of  $q_i$ , and the mass weighted fall velocity at the interface between grid-boxes. It is common in simple numerical schemes to assume that the values at the edges of the grid-box are the grid-box mean values. This is how ice sedimentation in the Met Office Unified Model is calculated but as noted earlier this assumption does not hold near the top of mixed-phase clouds. More advanced (2nd order) schemes interpolate between the values in two grid-boxes to give the appropriate values at the interface. This gives a more accurate estimate of the flux through the bottom of the grid-box, especially where the linear increase of ice water mixing ratio with depth down from cloud top continues through the top few grid-boxes. However, the depth of the layer over which the ice increases linearly is often 500 metres or less and therefore in coarse resolution models the grid-box mean values may not increase linearly with depth and the flux out of the uppermost model layer would be underestimated by a 2nd order scheme.

In order to give an accurate representation of the flux of ice from the uppermost cloudy grid-box, the value of ice water mixing ratio at the base of the layer is fixed at twice the grid-box mean quantity (consistent with the growth rate assumption) and the flux of ice out of this grid-box to the one below is calculated using this ice water mixing ratio. This is the same as a 2nd order scheme would do if the ice water mixing ratio continues increasing with depth beyond the uppermost grid-box but ensures the correct sedimentation of ice from the layer if the lower grid-box has a lower ice water mixing ratio.

The equation for calculating the mean fall speed is obtained by integrating the fall velocity of ice particles ( $v = aD^b$ ) over the assumed ice particle size distribution. This gives

$$v = \frac{c\Gamma(b+d+1)\rho^{-0.4}}{\Gamma(b+1)\left(\frac{aN_0\Gamma(b+1)}{\rho q_i}\right)^{\frac{d}{b+1}}}. \quad (17)$$

By increasing  $q_i$  to  $2q_i$ , the correct mean fall speed for the ice water mixing ratio found at the bottom of the grid-box can be calculated.

Next the flux through the bottom of the grid-box is increased by a factor to account for the larger amount of ice water mixing ratio to be fall to the grid box below. The factor is calculated as

$$\text{Factor} = 2 - \frac{v\Delta t}{\Delta z}. \quad (18)$$

This correction factor includes the factor of 2 increase of  $q_i$  at the bottom of the grid-box relative to the grid-box mean but also accounts for the decrease of  $q_i$  above the bottom of the grid-box and therefore reduces the correction factor by the fraction of the grid-box from which ice can fall to the grid-box beneath in a single timestep. Combining the fall speed increase and the flux increase gives an equivalent flux to the grid-box below as calculated in the high resolution model.

### 3.4. Representing liquid cloud structure

Unlike the ice water mixing ratio and supersaturation discussed so far, the liquid water content is not important for the calculation of any microphysical process rates in this model. They liquid water content is required for the radiation scheme and so an accurate representation of the grid-box mean water content and cloud fraction are required even when only part of the layer contains liquid water. To represent the sub-grid vertical structure of the cloud, the same assumption that the layer is well-mixed is used. This means that  $\theta_i$  and  $q_t$  are constant with height and  $T$  decreases approximately linearly with increasing height. If it is assumed that the liquid cloud is adiabatic and that the liquid water content linearly decreases from cloud top then the total liquid water content within the grid-box could be easily calculated. However, the inclusion of a diagnostic cloud scheme complicates this because nearer the cloud top there is both an increased (in-cloud) liquid water content and increased cloud fraction. Therefore, to correctly calculate the profile of liquid water, use of a cloud scheme is required. EMPIRE uses the simple Smith [1990] cloud scheme as explained in Part I of this paper, the same scheme as is implemented in the Met Office Unified Model when run over limited-area domains. It is fortunate that the  $Q_N$  (the grid-box mean saturation with respect to liquid normalised by the standard deviation of  $q_t$  within that grid-box) in this cloud scheme used to calculate both liquid water content and cloud fraction is an approximately linear function of height in a well-mixed layer.  $Q_N$  is defined as

$$Q_N = \frac{q_t - q_{sl}}{\sigma_s}, \quad (19)$$

where  $\sigma_s$  is the sub-grid standard deviation of  $q_t$ , defined as

$$\sigma_s = \frac{(1 - \text{RH}_{\text{crit}}) q_{sl}}{\sqrt{6}}. \quad (20)$$

The values of  $Q_N$  can be calculated at the top and bottom of the grid-box and the profile of  $Q_N$  can be assumed linear with height throughout the grid-box. Smith [1990] described how the liquid water mixing ratio ( $q_l$ ) and cloud fraction ( $CF$ ) are functions of  $Q_N$

$$\frac{q_l}{\sigma_s} = \begin{cases} 0 & Q_N \leq -\sqrt{6} \\ \frac{1}{\sqrt{6}} \left( 1 + \frac{Q_N}{\sqrt{6}} \right)^3 & -\sqrt{6} < Q_N \leq 0 \\ Q_N + \frac{1}{\sqrt{6}} \left( 1 - \frac{Q_N}{\sqrt{6}} \right)^3 & 0 < Q_N < \sqrt{6} \\ Q_N & \sqrt{6} \leq Q_N \end{cases} \quad (21)$$

$$CF = \begin{cases} 0 & Q_N \leq -\sqrt{6} \\ \frac{1}{2} \left( 1 + \frac{Q_N}{\sqrt{6}} \right)^2 & -\sqrt{6} < Q_N \leq 0 \\ 1 - \frac{1}{2} \left( 1 - \frac{Q_N}{\sqrt{6}} \right)^2 & 0 < Q_N < \sqrt{6} \\ 1 & \sqrt{6} \leq Q_N \end{cases} \quad (22)$$

These relationships can then be integrated over the depth of the grid-box (assuming  $\sigma_s$  is constant with height) to give accurate grid-box mean values of liquid water content and cloud fraction.

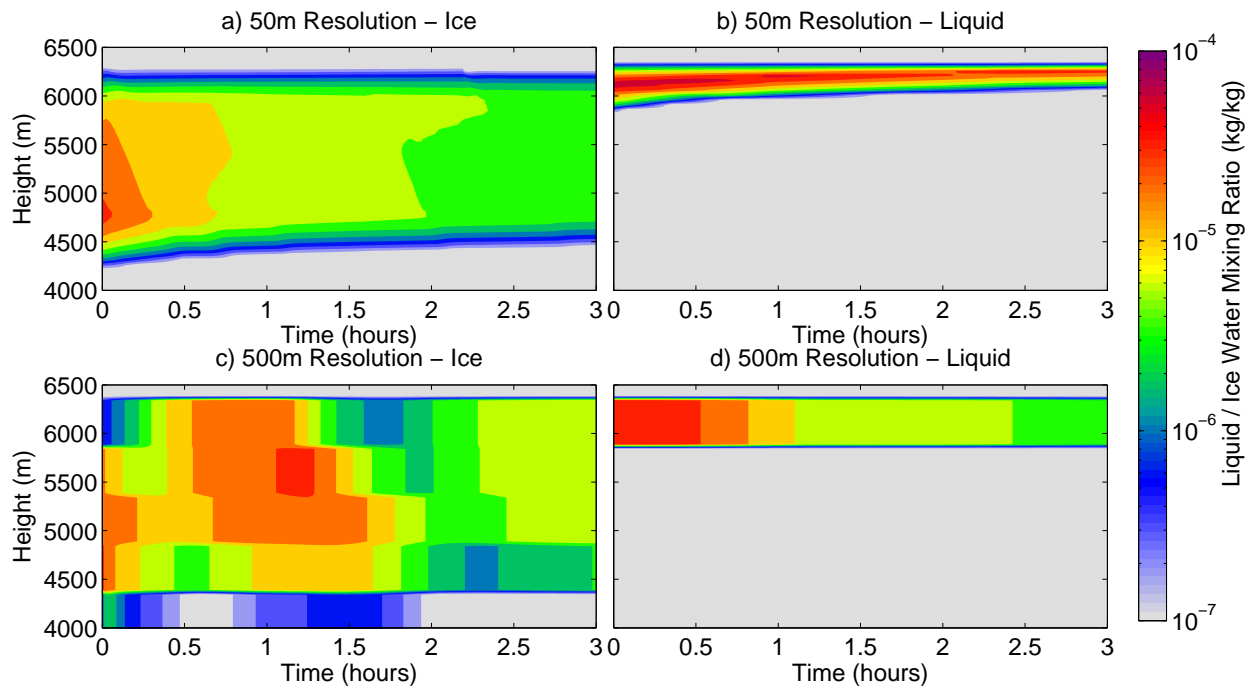


**Figure 5.** As figs. 3a-d but both simulations include the parameterization of the sub-grid vertical structure. Ice water mixing ratio is shown in the left hand panel and liquid water mixing ratio in the right hand panel. The colour bar is applicable to both liquid and ice.

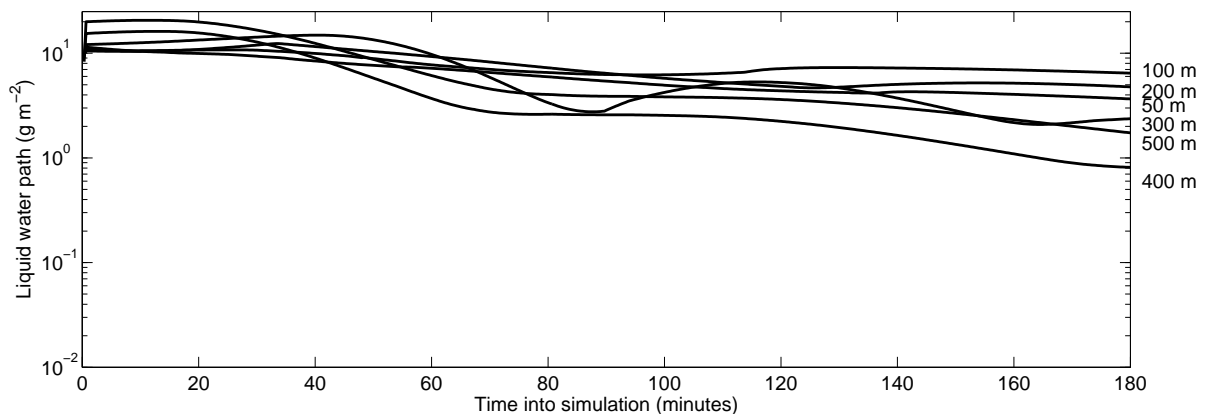


**Figure 6.** The evolution of simulated liquid water path with time for model vertical resolutions of 50–500-m from simulations where the vertical resolution parameterization is included. Compare this with figure 1 where no parameterization is included.

#### 4. Testing the parameterization

The parameterization has been tested in a number of simulations and scenarios to test its effect. First, idealised simulations at 50 and 500-m resolution are compared with each other and to the equivalent simulations without the vertical resolution parameterization. Then simulations spanning the range 50–500-m resolutions are investigated to check the simulations are now approximately resolution independent. Finally the parameterization is included in the simulations used in Part I of this paper, to confirm that the parameterization is beneficial in real case simulations as well as idealized simulation.

Adding the parameterization to the 50 and 500-m idealised simulations results in an increase in the liquid water content in both simulations. The liquid water content increases by a small amount (15%) in the 50-m simulation and by an order of magnitude in the 500-m simulation when averaged over the duration of each simulation (relative to

the control simulations without parameterization). The parameterization results in a reduction of mean ice water path of 5% in the 50-m simulation and an increase of 6% in the 500-m simulation; these values are much smaller than the changes to the liquid water paths in each simulation.

The vertical structure of the cloud in the coarse resolution simulations is much more similar to that of the fine resolution when the parameterization is included. Both simulations now have a thin layer of liquid water at cloud top persisting throughout the simulation (Fig. 5b,d) with the liquid water path of the cloud layer decreasing steadily with time. The ice water mixing ratio in the 500 metre simulation (Fig. 5c) takes longer to build up near cloud top, and reaches a lower peak value than the simulation with no parameterization; this enables the liquid water layer to persist for longer.

The parameterization has also been tested in simulations with vertical resolution spanning the range of 50 to 500 me-

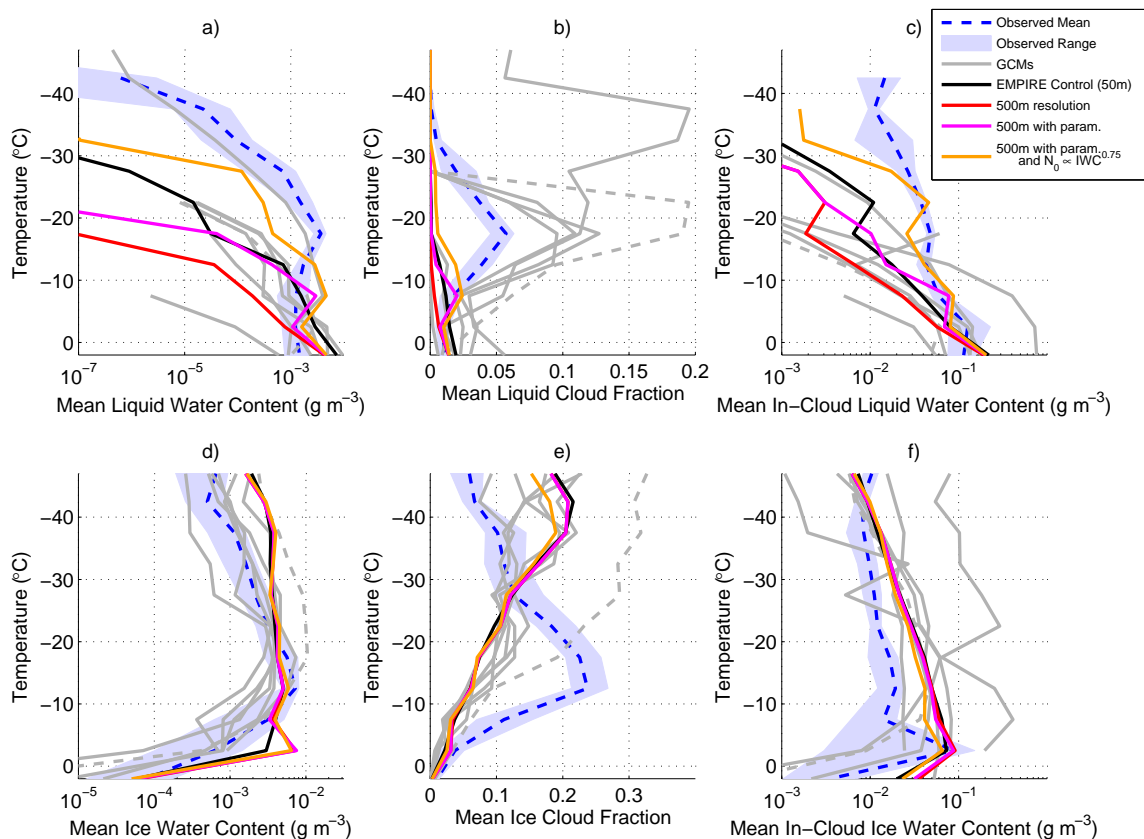


**Figure 7.** Mean liquid and ice water contents, cloud fractions and mean in-cloud water contents from EMPIRE experiments where the vertical resolution specification has been changed. The experiments are: (black) 50 metre vertical resolution, (red) 500 metre vertical resolution, (magenta) 500 metre vertical resolution with the sub-grid parameterization of cloud vertical structure active in the uppermost mixed-phase model level and (orange) the same as magenta but also including the ice particle size distribution change from Part I. The blue dashed line and light blue fill relate to remote sensing observations and the grey lines show the mean values predicted by a number of GCMs as plotted in Part I, Fig. 2.

tures. The inclusion of the parameterization results in an increase in the liquid water content for all vertical resolutions when averaged over the entire simulation (Fig. 6). There is now considerable agreement between the simulations of different vertical resolution about the persistence of the cloud layer and the liquid water path of the cloud at any given time. All resolutions up to 500 metres are able to maintain a supercooled liquid water layer throughout the simulation when the parameterization is included. This is a great improvement on the resolution dependence exhibited when no parameterization is included.

The parameterization has been tested in the 21 cases analysed in Part I of this paper. Running the simulations at 500 metre resolution showed that the mean supercooled liquid water content at temperatures below  $-5^{\circ}\text{C}$  reduced to just 12% of that in the 50 metre simulation (Fig. 7); with the parameterization included this increases to 84%. The distribution of supercooled liquid water as a function of height is comparable with the high resolution control simulation for temperatures warmer than  $-20^{\circ}\text{C}$  and almost an order of magnitude more liquid water at these temperatures than without the parameterization. Furthermore, inclusion of the change to the ice particle size distribution from Part I further increases the mean liquid water content, more consistent with observations.

This parameterization of the vertical gradients of ice water mixing ratio and supersaturation near the cloud top has removed much of the vertical resolution sensitivity for mixed-phase altocumulus clouds. The model is now capa-

ble of producing persistent mixed-phase layer cloud across a broad range of resolutions and the vertical structure is broadly similar for all resolutions tested.

## 5. Discussion

Simulations of mixed-phase altocumulus clouds using a single-column model have shown that coarse-resolution simulations are not able to maintain thin mixed-phase layers but that fine-resolution simulations can. In coarse-resolution simulations the supercooled liquid water at cloud top is converted to cloud ice too rapidly. In our idealised simulations, model vertical resolution of 100 m or finer is required before the simulations converge.

The resolution sensitivity arises because with coarse resolution the model is unable to represent the vertical gradients of ice water mixing ratio ( $q_i$ ) and temperature near the cloud top. The vertical gradient of temperature is important for diagnosing the vertical structure of supersaturation with respect to both liquid and ice. The ice supersaturation and ice water mixing ratio together control the rate of ice growth by vapour deposition. As models have only a single value for each prognostic variable within each grid-box the vertical gradients are usually ignored; however, calculating cloud properties and microphysical process rates from the layer-mean prognostic variables results in substantial errors in the case of mixed-phase altocumulus (Fig. 4).

A parameterization of the sub-grid vertical gradients at the top of mixed-phase altocumulus clouds has been developed. This parameterization assumes linear variations of  $q_i$

and temperature with height and calculates microphysical process rates and cloud properties using these profiles. Including this parameterization in the top model level of simulated mixed-phase clouds yields model simulations that are approximately resolution independent and are able to maintain persistent mixed-phase altocumulus clouds. The parameterization corrects the ice microphysical process rates near the cloud top, is not computationally expensive and greatly improves the representation of altocumulus in a coarse resolution single-column model and is suitable for inclusion in GCMs.

The resolution sensitivity accounts for a large fraction of missing supercooled liquid water found in models with prognostic ice cloud schemes (when compared to models where cloud ice is diagnosed, see Part I of this paper). The single-column model can now simulate persistent mixed-phase altocumulus clouds in a way that many GCMs cannot. The correction of such biases in GCMs, to allow persistent mixed-phase clouds, could alter the radiative transfer calculations within the model and will be important for both weather and climate prediction.

Our approach of single-column modelling with observational constraints has proved helpful to diagnose important biases in microphysical calculations and to fix them. The results presented in the two parts of this paper have highlighted errors in the simulation of mixed-phase altocumulus resulting from both ice particle size distribution errors (Part I) and vertical resolution sensitivity (Part II). The model simulations have much lower mean liquid water contents than observations. In general, any process that affects the ice growth rate is important for simulating mixed-phase clouds because the ice growth rate dominates the rate of conversion of liquid to ice and the rate at future times is dependent on the current ice water content.

The remaining difference of simulated liquid and ice cloud fraction from observations is of lesser importance and is a separate problem from the water contents as the clouds fractions are diagnosed from the water contents. Further work to evaluate model representations of the relationship between water content and cloud fraction, especially for ice, is ongoing.

Regarding the resolution sensitivity, the dependence of microphysical process rates on vertical gradients of cloud properties discussed in this paper explain why the model with the most sophisticated microphysics scheme evaluated in this study (the Met Office Unified Model) had a much lower mean liquid water content than the other models with more simple microphysics. Large underestimates of the supercooled liquid water content were present in model inter-comparisons of Arctic boundary-layer clouds [Klein *et al.*, 2009] and this parameterization might prove to reduce some of the bias in those simulations. Similar sensitivities were found when a new prognostic liquid and ice microphysics scheme was implemented in the ECMWF model, where substantial underestimates of supercooled liquid water were found in mixed-phase boundary-layer clouds resulting in large surface temperature biases [Forbes and Tompkins, 2011; Forbes and Ahlgrimm, 2014], specifically night time minimum temperatures over northern Europe in winter. A simple, artificial reduction of the ice growth rate in the upper portion of each cloud layer was implemented to address this problem; the sign of this change now seems physically justified given the vertical resolution sensitivity but it would be preferable to have the physics correctly represented. This sensitivity of surface temperature to the presence of supercooled liquid stresses the importance of correctly predicting mixed-phase clouds for weather forecasting as well as better representing cloud feedbacks important for our future climate. Further work is now required to implement this parameterization in climate models and to provide a revised estimate of cloud feedbacks and climate sensitivity.

**Acknowledgments.** The first author was supported by a PhD studentship from the Natural Environment Research Council (NERC). We thank Stephen Belcher, Daniel Kirshbaum and Paul Field for useful discussions throughout the course of this work.

## References

- Andrews T, Gregory JM, Webb MJ, Taylor KE. 2012. Forcing, feedbacks and climate sensitivity in CMIP5 coupled atmosphere-ocean climate models. *Geophys. Res. Lett.* **39**: L09712, doi:10.1029/2012GL051607.
- Barrett AI, Hogan RJ, Forbes RM. 2014. Why are mixed-phase altocumulus clouds poorly predicted by large-scale models? Part I: Poorly represented physical processes. *J. Geophys. Res.* .
- Bony S, Colman R, Kattsov VM, Allan RP, Bretherton CS, Dufresne JL, Hall A, Hallegatte S, Holland MM, Ingram W, Randall DA, Soden BJ, Tselioudis G, Webb MJ. 2006. How well do we understand and evaluate climate change feedback processes? *J. Clim.* **19**: 3445–3482.
- Edwards JM, Slingo A. 1996. Studies with a flexible new radiation code. I: Choosing a configuration for a large-scale model. *Q. J. R. Meteorol. Soc.* **122**: 689–719.
- Fleishauer RP, Larson VE, Vonder Haar TH. 2002. Observed microphysical structure of midlevel, mixed-phase clouds. *J. Atmos. Sci.* **59**: 1779–1804.
- Forbes RM, Ahlgrimm M. 2014. An improved representation of high-latitude boundary layer mixed-phase cloud in the ECMWF global model. *Submitted to Mon. Wea. Rev.*
- Forbes RM, Tompkins A. 2011. An improved representation of cloud and precipitation. *ECMWF Newsl.* **129**: 1318.
- Hobbs PV, Rangno AL. 1985. Ice particle concentrations in clouds. *J. Atmos. Sci.* **42**: 2523–2549.
- Hogan RJ, Francis PN, Flentje H, Illingworth AJ, Quante M, Pelon J. 2003. Characteristics of mixed-phase clouds: Part I: Lidar, radar and aircraft observations from CLARE'98. *Q. J. R. Meteorol. Soc.* **129**: 2089–2116.
- Illingworth AJ, Hogan RJ, O'Connor EJ, Bouniol D, Brooks ME, Delanoë J, Donovan DP, Gaussiat N, Goddard JWF, Haefelin M, Baltink HK, Krasnov OA, Pelon J, Piriou JM, Protat A, Russchenberg HWJ, Seifert A, Tompkins AM, van Zadelhoff GJ, Vinit F, Willen U, Wilson DR, Wrench CL. 2007. Cloudnet - continuous evaluation of cloud profiles in seven operational models using ground-based observations. *Bull. Amer. Meteor. Soc.* **88**: 885–898.
- Klein SA, McCoy RB, Morrison H, Ackerman AS, Avramov A, de Boer G, Chen M, Cole JNS, Del Genio AD, Falk M, Foster MJ, Fridlind A, Golaz JC, Hashino T, Harrington JY, Hoose C, Khairoutdinov MF, Larson VE, Liu X, Luo Y, McFarquhar GM, Menon S, Neggers RAJ, Park S, Poellot MR, Schmidt JM, Sednev I, Shipway BJ, Shupe MD, Spangenberg DA, Sud YC, Turner DD, Veron DE, von Salzen K, Walker GK, Wang Z, Wolf AB, Xie S, Xu KM, Yang F, Zhang G. 2009. Intercomparison of model simulations of mixed-phase clouds observed during the ARM Mixed-Phase Arctic Cloud Experiment. I: Single-layer cloud. *Q. J. R. Meteorol. Soc.* **135**(641): 979–1002, doi:10.1002/qj.416.
- Lock AP, Brown AR, Bush MR, Martin GM, Smith RNB. 2000. A new boundary layer mixing scheme. Part I: Scheme description and single-column model tests. *Mon. Wea. Rev.* **128**: 3187–3199.
- Louis JF. 1979. A parametric model of vertical eddy fluxes in the atmosphere. *Bound.-Layer. Meteor.* **17**: 187–202.
- McFarquhar GM, Zhang G, Poellot MR, Kok GL, McCoy R, Tooman T, Fridlind A, Heymsfield A. 2007. Ice properties of single-layer stratocumulus during the Mixed-Phase Arctic Cloud Experiment: 1. Observations. *J. Geophys. Res.* **112**: D24201.
- Mitchell JFB, Senior CA, Ingram WJ. 1989. CO<sub>2</sub> and climate: a missing feedback? *Nature* **341**: 132–134.
- Morrison H, de Boer G, Feingold G, Harrington J, Shupe MD, Sullia K. 2012. Resilience of persistent arctic mixed-phase clouds. *Nature Geoscience* **5**: 11–17.
- Pruppacher HR, Klett JD. 1978. *Microphysics of clouds and precipitation*. D. Reidel Publishing Company, Boston, USA.

- Rauber RM, Tokay A. 1991. An explanation for the existence of supercooled water at the top of cold clouds. *J. Atmos. Sci.* **48**: 1005–1023.
- Senior CA, Mitchell JFB. 1993. Carbon dioxide and climate: The impact of cloud parameterization. *J. Clim.* **6**: 393–418.
- Shupe MD, Daniel J, de Boer G, Eloranta EW, Kollias P, Long CN, Luke EP, Turner DD, Verlinde J. 2008. A focus on mixed-phase clouds. *Bull. Amer. Meteor. Soc.* **89**: 1549–1562.
- Shupe MD, Matrosov SY, Uttal T. 2006. Arctic mixed-phase cloud properties derived from surface-based sensors at SHEBA. *J. Atmos. Sci.* **63**: 697–711.
- Smith AJ, Larson VE, Niu J, Kankiewicz JA, Carey LD. 2009. Processes that generate and deplete liquid water and snow in thin midlevel mixed-phase clouds. *J. Geophys. Res.* **114**: D12203.
- Smith RNB. 1990. A scheme for predicting layer clouds and their water content in a general circulation model. *Q. J. R. Meteorol. Soc.* **116**: 435–460.
- Tsushima Y, Emori S, Ogura T, Kimoto M, Webb MJ, Williams KD, Ringer MA, Soden BJ, Li B, Andronova N. 2006. Importance of the mixed-phase cloud distribution in the control climate for assessing the response of clouds to carbon dioxide increase: a multi-model study. *Clim. Dyn.* **27**: 113–126.
- Verlinde J, Harrington JY, McFarquhar GM, Yannuzzi VT, Avramov A, Greenberg S, Johnson N, Zhang G, Poellot MR, Mather JH, Turner DD, Eloranta EW, Zak BD, Prenni AJ, Daniel JS, Kok GL, Tobin DC, Holz R, Sassen K, Spangenberg D, Minnis P, Tooman TP, Ivey MD, Richardson SJ, Bahrman CP, Shupe M, DeMott PJ, Heymsfield AJ, Schofield R. 2007. The Mixed-Phase Arctic Cloud Experiment. *Bull. Amer. Meteor. Soc.* **88**: 177–190.
- Wilson RW, Ballard SP. 1999. A microphysically based precipitation scheme for the UK Meteorological Office Unified Model. *Q. J. R. Meteorol. Soc.* **125**: 1607–1636.
- Zhang D, Wang Z, Liu D. 2010. A global view of midlevel liquid-layer topped stratiform cloud distribution and phase partition from calipso and cloudsat measurements. *J. Geophys. Res.* **115**: D00H13.
- Zhang MH, Lin WY, Klein SA, Bacmeister JT, Bony S, Cederwall RT, Genio ADD, Hack JJ, Loeb NG, Lohmann U, Minnis P, Musat I, Pincus R, Stier P, Suarez MJ, Webb MJ, Wu JB, Xie SC, Yao MS, Zhang JH. 2005. Comparing clouds and their seasonal variations in 10 atmospheric general circulation models with satellite measurements. *J. Geophys. Res.* **110**: D15S02.
- Zuidema P, Baker B, and J Intrieri YH, Key J, Lawson P, Matrosov S, Shupe M, Stone R, Uttal T. 2005. An arctic springtime mixed-phase cloudy boundary layer observed during SHEBA. *J. Atmos. Sci.* **62**: 160–176.

---

Corresponding author: Andrew. I. Barrett, Department of Meteorology, University of Reading, Reading, RG6 6BB, UK. (a.i.barrett@reading.ac.uk)